Influence of hydrostatic pressure on the bulk magnetic properties of Eu_{2}Ir_{2}O_{7}

G. Prando, R. Dally, W. Schottenhamel, Z. Guguchia, S.-H. Baek, R. Aeschlimann, A. U. B. Wolter, S. D. Wilson, B. Büchner, and M. J. Graf

Phys. Rev. B **93**, 104422 — Published 28 March 2016

DOI: 10.1103/PhysRevB.93.104422

Influence of hydrostatic pressure on the bulk magnetic properties of $Eu_2Ir_2O_7$

G. Prando,[1,2,*] R. Dally,[3] W. Schottenhamel,[2] Z. Guguchia,[4] S.-H. Baek,[2]
R. Aeschlimann,[2] A. U. B. Wolter,[2] S. D. Wilson,[5] B. Büchner,[2,6] and M. J. Graf[3]

[1] *Center for Transport and Devices of Emergent Materials, Technische Universität Dresden, D-01062 Dresden, Germany*
[2] *Leibniz-Institut für Festkörper- und Werkstoffforschung (IFW) Dresden, D-01171 Dresden, Germany*
[3] *Department of Physics, Boston College, Chestnut Hill, Massachusetts 02467, USA*
[4] *Laboratory for Muon Spin Spectroscopy, Paul Scherrer Institut, CH-5232 Villigen PSI, Switzerland*
[5] *Department of Materials, University of California, Santa Barbara, California 93106, USA*
[6] *Institut für Festkörperphysik, Technische Universität Dresden, D-01062 Dresden, Germany*

(Dated: March 3, 2016)

We report on the magnetic properties of $Eu_2Ir_2O_7$ upon the application of hydrostatic pressure P by means of macroscopic and local-probe techniques. In contrast to previously reported resistivity measurements, our dc magnetization data unambiguously demonstrate a non-monotonic dependence of T_N, i. e., the critical transition temperature to the magnetic phase, on P. Strikingly, the recently calculated behaviour for T_N closely reproduces our results under the assumption that P lowers the U/W ratio (i. e., Coulomb repulsion energy over electronic bandwidth). Zero-field muon-spin spectroscopy measurements confirm that the Ir^{4+} magnetic moment and/or the local magnetic configuration are only weakly perturbed by low P values. Accordingly, our current experimental findings strongly support the preservation of a 4-in/4-out ground state across the accessed region of the phase diagram.

PACS numbers: 62.50.-p, 71.30.+h, 75.40.Cx, 76.75.+i

I. INTRODUCTION

The arrangement of magnetic moments at the vertices of a pyrochlore lattice (i. e., a geometrically-frustrating crystalline structure composed of corner-sharing tetrahedra) leads to a great variety of exotic electronic ground states for $R_2M_2O_7$ materials.[1] One important finding common to several families of these oxides is that changes in r_I, the ionic radius of the rare-earth ion R^{3+}, gradually tune the local crystalline environment around the transition metal ion M^{4+} and the overall electronic behaviour of the compound in turn. This is verified for M ions belonging to the $4d$ (e. g., Mo)[2,3] and $5d$ (e. g., Ir)[4–7] groups. Here, the characteristic temperature $T_{\rm MI}$ for the development of a MIT (metal-to-insulator transition) is directly controlled by the average value $\langle r_I \rangle$ related to a gradual $R_{1-x}R'_x$ substitution.[8–11] However, a chemical dilution is generally delicate to handle as it necessarily introduces a non-negligible degree of quenched disorder, possibly detrimental for most of the intrinsic physical properties under investigation. Moreover, R ions may also be characterized by localized magnetic moments arising from their incomplete f electronic shells and this fact may influence measurements when the actual magnetic properties are being studied.

These latter aspects are particularly relevant as the MIT in $R_2Mo_2O_7$ and $R_2Ir_2O_7$ is associated with a dramatic change in the magnetic behaviour as well. Antiferromagnetic insulating and metallic paramagnetic states compose indeed the two main regions of the EPD (electronic phase diagram) of Ir-based pyrochlores,[5] even if this is only a very simplistic description. Theory predicts that comparable energy scales for the Coulomb repulsion U and the spin-orbit coupling make the EPD of pyrochlore iridates extremely rich with exotic states. In the insulating regime, a non-collinear state is theoretically predicted[12–14] and experimentally claimed[15,16] for Ir^{4+} magnetic moments, pointing along the local $\langle 111 \rangle$ directions all inside or all outside the tetrahedron at whose vertices they sit (4-in/4-out configuration). Theory suggests that such an arrangement is necessary for the achievement of topologically non-trivial properties such as, e. g., the Weyl semimetallic phase.[12,17]

A cleaner structural approach in order to fine-tune the ground state of the system is to vary P (external pressure). This method has been very successful for M = Mo[18–21] and, more recently, for the case of Ir[22,23] where P gradually suppresses the insulating state and triggers metallicity in several compounds.[11,23] Transport properties have been mainly discussed in the literature and, although the trend is clear, a purely metallic phase is never properly achieved. Moreover, discrepancies exist among the results for different compounds. While $T_{\rm MI}$ is clearly sensitive to pressure for $Sm_2Ir_2O_7$, $Nd_2Ir_2O_7$, and $Pr_2Ir_2O_7$ (and intermediate compositions),[11] no sizeable effect of P is reported for this quantity in $Eu_2Ir_2O_7$.[23] Finally, a detailed investigation of the magnetic properties of these compounds under P is still missing.

In this paper we focus on the magnetic properties of $Eu_2Ir_2O_7$ under pressure, both from macroscopic (dc magnetometry) and local (μ^+SR, muon-spin spectroscopy) perspectives. The absence of a localized magnetic moment from f shells in $Eu_2Ir_2O_7$ is a great advantage in the study of the intrinsic magnetic properties of the Ir sublattice. From our magnetization measurements, we deduce a clearly non-monotonic P-dependence

of T_N pointing to its departure from $T_{\rm MI}$.[23] Strikingly, the behaviour recently reported for T_N from relativistic LDA (local density approximation) + DMFT (dynamical mean-field theory) calculations[24] closely reproduces our data under the assumption that P influences the U/W ratio (W representing the electronic bandwidth). At the same time, ZF (zero-field) μ^+SR data confirm that the Ir^{4+} magnetic moment and/or the local magnetic configuration are only weakly perturbed by pressure in the $P \lesssim 24$ kbar range. Accordingly, our measurements strongly support the preservation of a 4-in/4-out ground state across the whole accessed magnetic region of the phase diagram.

II. EXPERIMENTAL DETAILS

A. Sample synthesis

Stoichiometric amounts of Eu_2O_3 (Alfa 99.99 %) and IrO_2 (Alfa 99.99 %) were mixed and sintered at 800 °C for 15 hours, 1000 °C for 100 hours, and 1100 °C for 100 hours. The powder was mixed and pelletized with an isostatic cold press in between each sintering step. The sample purity was tested via laboratory XRD (x-ray diffraction) measurements in a Brucker D2 Phaser system. Other than a small impurity fraction of ~ 1 % Ir, powder diffraction data (see Fig. 1) revealed a phase pure specimen of $Eu_2Ir_2O_7$.

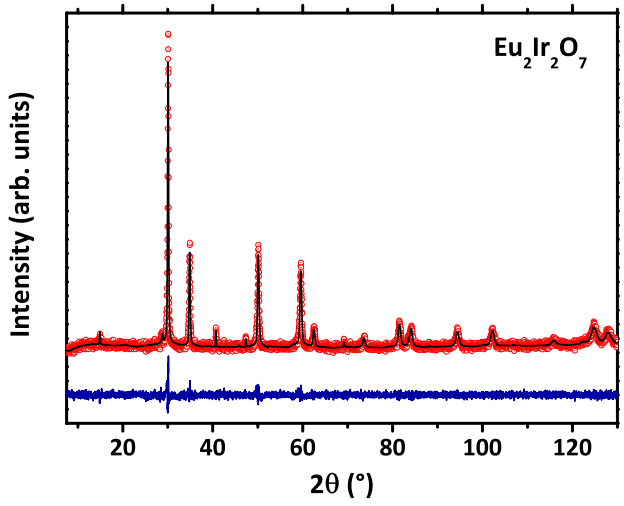

FIG. 1: (Color online) Powder XRD diffractogram for the currently investigated $Eu_2Ir_2O_7$ sample (experimental data are presented as red circles) together with the relative best-fits after a Rietveld analysis (black line). The blue line shows the residuals after subtraction of data and fit.

B. dc magnetometry

We performed measurements of M (dc magnetization) for temperature values 2 K $\leq T \leq$ 150 K by means of a commercial Magnetic Property Measurement System magnetometer (Quantum Design) based on a superconducting quantum interference device. We employed a home-made CuBe PC (pressure cell) in order to apply P. Here, two opposing cone-shaped ceramic anvils compress a CuBe gasket with a cylindrical hole used as sample chamber.[25,26] The uniaxial force F is applied at ambient temperature and it is converted into hydrostatic pressure in the sample chamber by a homogeneous mixture of ethanol (1 part) and methanol (4 parts). This choice for the transmitting medium is among the best ones in order to keep the degree of non-hydrostaticity as low as possible within the accessed P range.[27] We employed two different disk-shaped CuBe gaskets with sample space diameter $\varnothing = 0.8$ mm and $\varnothing = 0.4$ mm currently allowing us to reach maximum pressure values ~ 21 kbar and ~ 42 kbar, respectively. In the case of the former setup, we performed measurements with Daphne oil 7373 as transmitting medium as well, allowing us to achieve slightly higher maximum P values (~ 23 kbar).

In all the cases mentioned above, we checked the P value and its homogeneity at low temperature by measuring the FC (field-cooling) diamagnetic response associated with the superconducting transition of a small Pb manometer inserted in the sample space. We performed these measurements upon the application of a small magnetic field $H = 10$ Oe. Transition widths $\lesssim 0.1$ K denote good P homogeneity at all the investigated P values (see Fig. 2). Accordingly, the P value at low T was estimated from the expression[28]

$$P = \frac{7.17 - T_c}{0.0361} \left[\frac{\rm K}{\rm K \times kbar^{-1}} \right], \qquad (1)$$

T_c being the measured mid-point of the diamagnetic transition. Measurements of $Eu_2Ir_2O_7$ were then performed at the fixed value $H = 1$ kOe, always by warming the sample after a FC protocol and (for most of them) upon gradually increasing P. The full reversibility of the observed P dependence was checked and verified while unloading the PC, both for the Pb transition and for the actual magnetic properties of the sample.

As is observed in Fig. 2, a T-dependent magnetic background is detected in our M measurements arising from the PC itself. Accordingly, we describe in Appendix A how the overall M was analyzed in order to disentangle the background from the intrinsic signal from the sample.

C. μ^+ spin spectroscopy

We performed μ^+SR measurements[29,30] at the SμS muon source (Paul Scherrer Institut, Switzerland) on the GPS and GPD spectrometers (πM3 and μE1 beamlines,

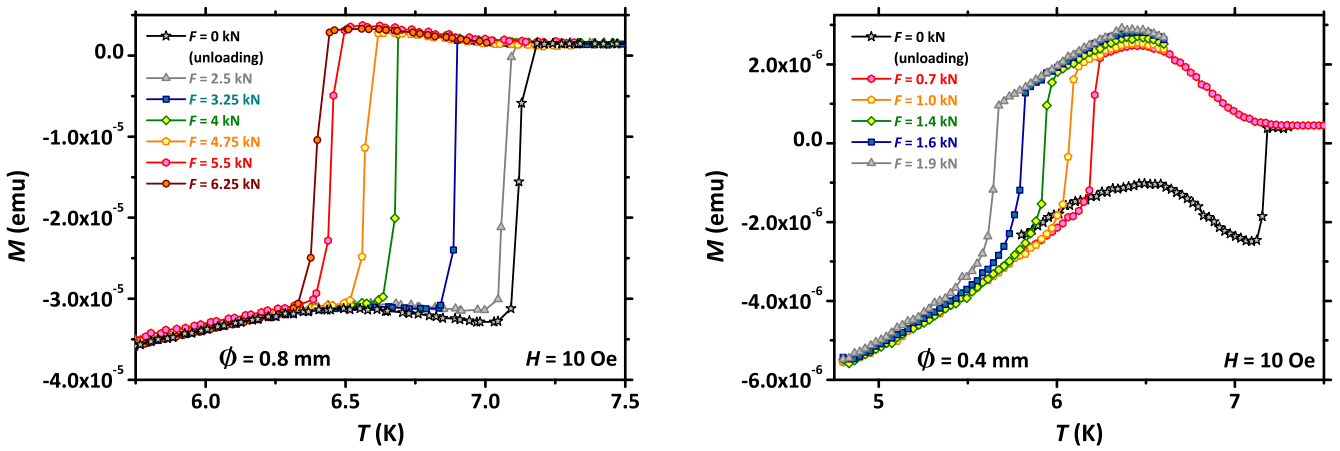

FIG. 2: (Color online) Superconducting transitions of the Pb manometer for the gaskets with sample chamber diameter $\varnothing = 0.8$ mm (left panel) and $\varnothing = 0.4$ mm (right panel). The different curves correspond to different applied forces (see legend). The sudden jump in magnetization is ascribed to the diamagnetic contribution from the superconducting phase and its overall width is safely below 0.1 K for all the applied forces, denoting a good pressure homogeneity within the whole accessed experimental P range. The actual P values were quantified from Eq. (1). The other source of T-dependence for M is the background signal from the PC, different for the two employed setups.

respectively) for 5 K $\leq T \leq$ 200 K, in ZF conditions. We applied external pressures at ambient T by means of a double-wall piston-cylinder PC made of MP35N alloy. The transmitting medium Daphne oil 7373 assured nearly-hydrostatic P conditions in the whole experimental range. The P value and its homogeneity were checked at low T. In particular, the diamagnetic response associated with the superconducting transition of a small In wire in the sample space was measured by means of ac susceptibility (not shown). The data analysis is discussed in great detail in the Supplementary Material.[31]

III. RESULTS

A. Sample characterization at ambient P

We performed a thorough characterization of electrical transport and magnetic properties of the sample at ambient pressure. We have reported the main results in the Supplementary Material.[31]

B. dc magnetometry under pressure

Representative results for the magnetic susceptibility $\chi_m = M_m/H$ in molar formula units at the different investigated P values are shown in Fig. 3. We define the transition temperature T_N to the LRO (long-range ordered) phase from the kink-like anomaly in $M(T)$ (see the double-linear fitting procedure graphically shown in the insets of Fig. 3). We also define the amount of FC susceptibility associated with the magnetic phase upon investigation as $\Delta\chi_m = \chi_m(25\text{ K}) - \chi_m(T_N)$ (see the left panel of Fig. 3). The choice of $T = 25$ K is due to residual extrinsic background contributions from the pressure cell preventing us from fully exploiting measurements at lower T values. However, $T = 25$ K is safely in the saturation regime for M at ambient P.[31]

We distinguish between two qualitatively different regimes for $Eu_2Ir_2O_7$ under P (see Fig. 3). For $P \lesssim 20$ kbar, both T_N and $\Delta\chi_m$ increase with increasing P, while for $P \gtrsim 25$ kbar both quantities decrease. The situation is summarized later on in Fig. 6, where the actual P dependence of both T_N and $\Delta\chi_m$ is reported. T_N exhibits a smooth and continuous dependence on P clearly passing through a maximum at $P \sim 20 - 25$ kbar. While the crossover between the two regimes in $\Delta\chi_m$ is marked by a discontinuity whose origin could be accounted for by an instrumental artefact,[38] the observation of a qualitatively different behaviour of $\Delta\chi_m$ for $P \lesssim 20$ kbar and $P \gtrsim 25$ kbar is unambiguous.

C. μ^+SR under pressure

In order to investigate the effect of P on the magnetic moments at the microscopic level, we performed ZF-μ^+SR experiments for $P \lesssim 24$ kbar (i. e., the current maximum value achievable by the employed setup). We show representative raw data for the ZF μ^+ spin depolarization in the time domain in the inset of Fig. 4. Continuous lines are best-fitting curves according to a standard treatment of ZF-μ^+SR data for magnetic materials.[31] The well-defined spontaneous magnetic field at the muon site $B_{\mu 1}$ is indicative of a LRO magnetic phase,[34,39] resulting in the coherent oscillations shown in the inset of Fig. 4. The characteristic frequency $\nu_{\mu 1}$ is directly proportional to the order parameter of the magnetic transition and, in the current case, to the magnetic moment

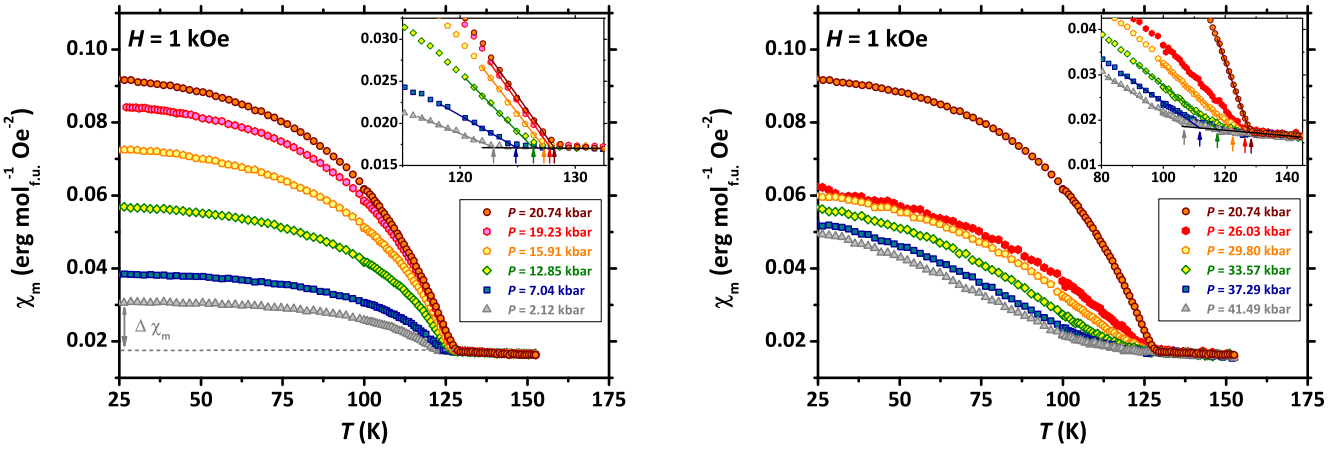

FIG. 3: (Color online) Main panels: T dependence of the FC susceptibility χ_m for $P \lesssim 20$ kbar and $P \gtrsim 20$ kbar after background subtraction (left and right panel, respectively). The amount of FC susceptibility at 25 K related to the magnetic phase of $Eu_2Ir_2O_7$ is defined as $\Delta\chi_m$ (see the graphical definition in the left panel). The insets display enlargements of the magnetic transition region together with the double-linear fits defining the actual T_N values (arrows).

of Ir^{4+} ions.[31] From this, we can confirm that no drastic qualitative changes are induced by P in the Ir^{4+} magnetic moment and/or in the 4-in/4-out configuration up to ~ 24 kbar.

A closer examination of data[40] reveals other features, better visualized in the main panel of Fig. 4 by FFT (fast Fourier transform) of the signal. A gradual increase of the transversal relaxation, i. e., the oscillations' damping, is observed upon increasing P. Accordingly, this is reflected in a progressive broadening of the FFT spectra. We relate this effect to the inevitable progressive increase in P inhomogeneity within a powder sample with increasing P, rather than to any intrinsic effect. At the same time, $B_{\mu 1}^{\rm sat}$ (i. e., the local field at the muon site in saturation) is continuously shifted to lower values upon increasing P. For the aim of clarity, we summarize these latter data in Fig. 5, clearly showing a linear dependence on P. The smoothness of the $B_{\mu 1}^{\rm sat}$ vs. P trend denotes the absence of any dramatic magnetic or structural effect induced by P. Remarkably, we also notice that the relative variation is tiny $[\Delta B_{\mu 1}^{\rm sat}/B_{\mu 1}^{\rm sat}(0) \sim 3$ % at the maximum $P]$ and this aspect is not consistent at all with any appreciable change in the Ir^{4+} moment or a change from the 4-in/4-out magnetic configuration. In particular, the observed behaviour could be well explained by a gradual modification in the lattice parameters gradually

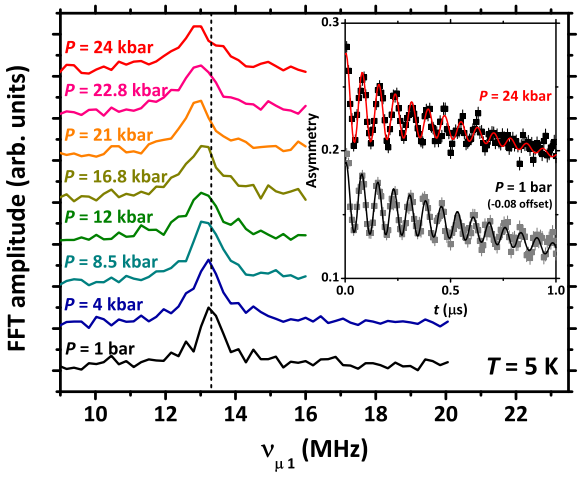

FIG. 4: (Color online) Main panel: FFT of the μ^+ time ZF-depolarizations (representative data are shown in the inset together with their best-fitting curves) measured on the GPD spectrometer at fixed temperature in the saturation regime. The vertical dashed line is a guide-to-the-eye indicating the central frequency at ambient P.

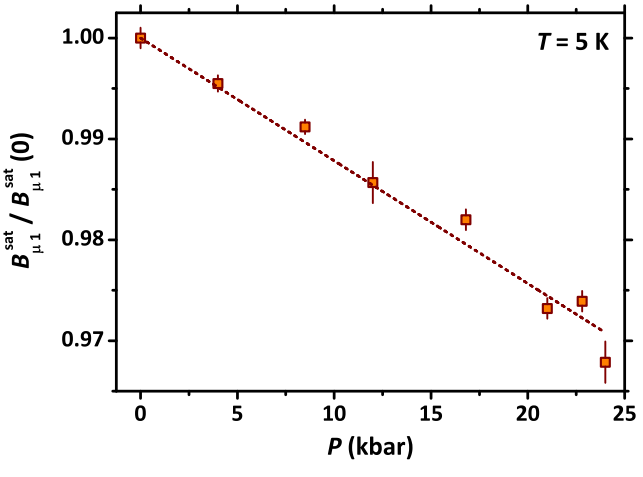

FIG. 5: (Color online) Local magnetic field at the muon site [normalized to its value $B_{\mu 1}^{\rm sat}(0) = 977.4$ G at ambient pressure] reported as a function of P after the fitting procedure to experimental ZF time-depolarization curves (see the inset of Fig. 4). The dashed line is a linear best-fitting curve to experimental data.

influencing the muon implantation site and the probed dipolar magnetic field in turn.[32] This argument should be substantiated by *ab-initio* calculations of the muon implantation site[16,41,42] and by a detailed measurement of the structural parameters of this current sample under comparable P conditions.

IV. DISCUSSION

Remarkably, the non-monotonic behaviour of T_N measured by means of dc magnetometry is highly reminiscent of what was recently calculated by means of relativistic LDA-DMFT for the analogue material $Y_2Ir_2O_7$.[24] In the current case of $Eu_2Ir_2O_7$, we exploit the presence of Eu^{3+} at the R site (i.e., a non-magnetic ion such as Y^{3+}) allowing us to neglect any f–d interaction[43] which, although interesting on its own, could in principle hide the intrinsic magnetic properties of the Ir sublattice. We report here data from the calculated EPD[24] superimposed to our experimental results (see the dashed red line in Fig. 6). While the absolute values for the calculated T_N are clearly overestimating the experimental result (an issue associated by Shinaoka *et al.* with the neglecting "of spatial fluctuations in the DMFT approximation" – see Ref. 24), these can be rescaled by an empirical factor ~ 3.15 under the constraint that the scale zero matches the experimental one. Results clearly display a striking agreement with our measurements under the assumption that increasing P is reducing the U/W ratio. We stress that only changes in U are actually considered in the LDA-DMFT calculations with fixed W value.[24] However, one physically expects that P influences both U and W and that, at the same time, the sensitivity of W to P is much higher than that of U.

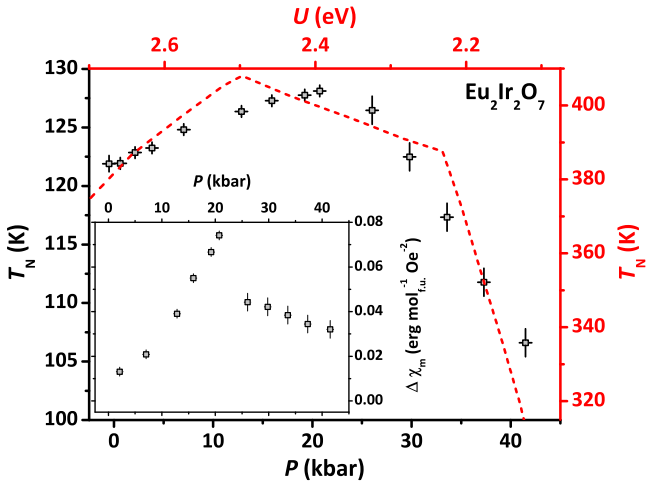

FIG. 6: (Color online) Main panel: P dependence of the critical transition temperature (squares, bottom and left scales). The red dashed line (top and right scales) is obtained by digitizing data of the calculated EPD discussed in Ref. 24. The right scale has been rescaled so that the scale zero coincides with that of the left scale. Inset: P dependence of the FC susceptibility $\Delta\chi_m$ in the magnetic phase.

Several interesting observations follow from the results presented above. First of all, the substantial agreement of the experimental and calculated EPDs allows us to rule out that the non-monotonic trend observed for T_N is arising from, e. g., P-induced structural phase transitions at $P \sim 25$ kbar but rather points towards an intrinsic underlying electronic mechanism. At the same time, by considering the investigation of transport properties reported in Ref. 23, we notice a possible departure of $T_{\rm MI}$ and T_N under P which would solve the current controversy between Mott- vs. Slater-character of the transition in favour of the former. In fact, Tafti *et al.* report that $T_{\rm MI}$ is mostly unaffected by P up to ~ 120 kbar,[23] contrasting with our current reports on T_N. However, we stress that the two current datasets are associated with two different samples, making the current direct comparisons difficult. We also stress that, within the framework of Ref. 24, one has $T_{\rm MI} = T_N$ over the whole phase diagram. Overall, it would be clearly very interesting to extend dc magnetometry measurements to higher P values.

The behaviour of $\Delta\chi_m$ vs. P needs to be commented further as well. We argue that the initial ($P \lesssim 20$ kbar) fast rise of $\Delta\chi_m$ could be due to two different phenomena. On the one hand, P may be inducing different configurations for magnetic domains whose DWs (domain walls) would carry non-trivial exotic properties together with a net magnetization, according to recent theoretical proposals.[44] However, our finding of a LRO phase with non-zero local magnetic field over a bulk fraction of the sample (see below) fails to verify the prediction of a vanishing uniform magnetization in the bulk.[44] Another possible scenario is a gradual modification of the crystalline environment of Ir under P slightly departing from the ideal cubic symmetry. This would imply an increasing degree of canting for the Ir^{4+} magnetic moments, possibly resulting in an increased magnetic susceptibility in the presence of an external magnetic field. The subsequent decrease of $\Delta\chi_m$ with further increasing P ($P \gtrsim 25$ kbar) can be again understood from Ref. 24 as an actual decrease of the Ir^{4+} magnetic moment, whose reduction develops in the same region of the fast suppression of T_N. Unfortunately, the current setup for μ^+SR measurements at the GPD facility does not allow us to reach higher P values, which would locally verify the suppression of the Ir^{4+} magnetic moment in that P range.

It is worth emphasizing that our experimental validation of the trend calculated in Ref. 24 suggests a direct verification of other important conclusions of that study. In particular, quite indirectly, our data support a highly hybridized state between the $j_{\rm eff} = 1/2$ and $j_{\rm eff} = 3/2$ manifolds.[24] Finally, we also confirmed previous observations by Ishikawa *et al.*[37] about the absence of any thermal hysteresis across T_N (not shown), characterizing the phase transition as second-order. This is also in good agreement with the results in Ref. 24 where the first-order character of the transition is reported only very close to

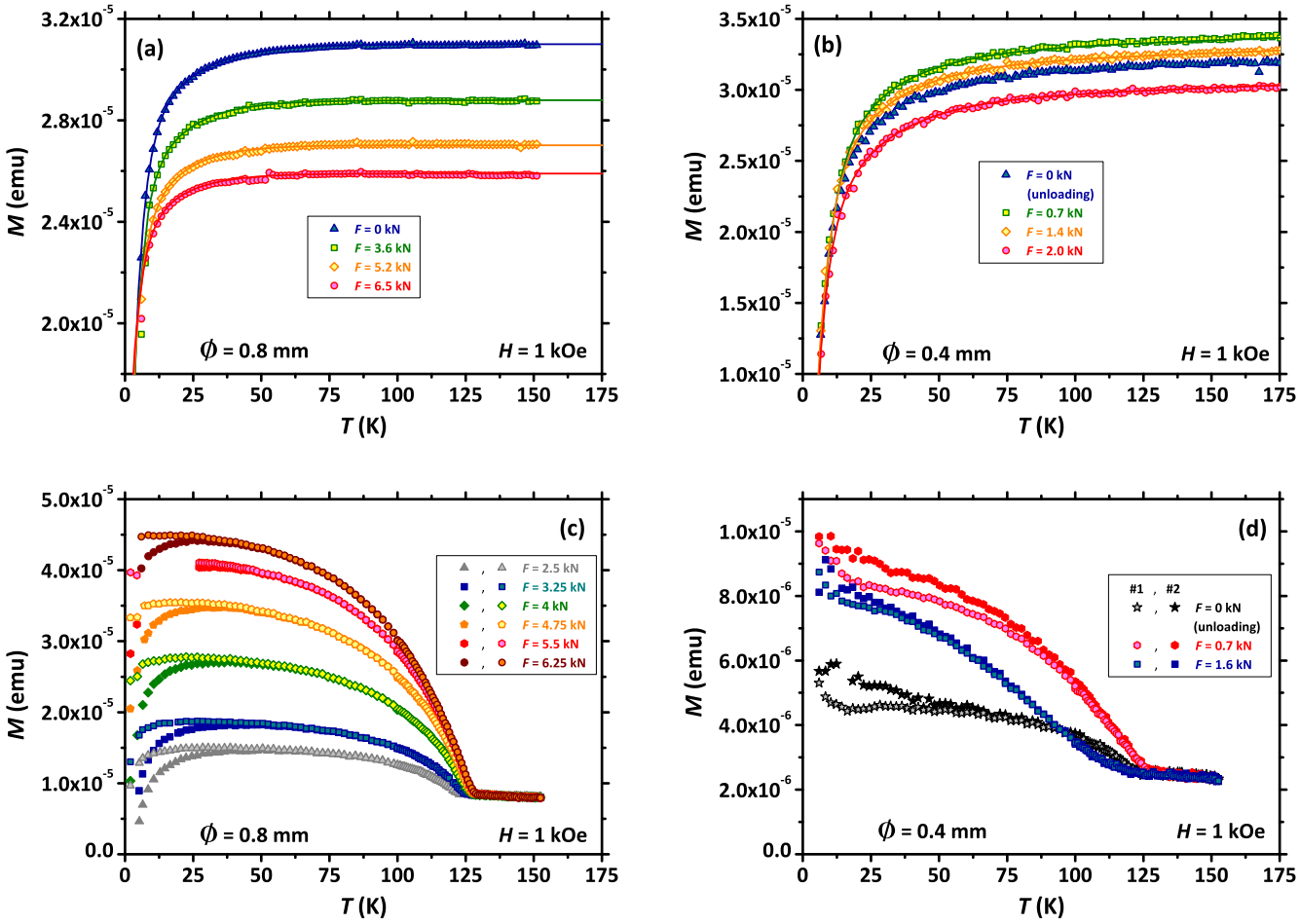

FIG. 7: (Color online) Representative results of the background subtraction procedure for the magnetization data for both employed setups. The procedure and the meaning of the different symbols are explained in the text below.

the full disruption of the antiferromagnetic ground state.

V. CONCLUSIONS

Summarizing, in this paper we focussed on the magnetic properties of $Eu_2Ir_2O_7$ under P reporting on an unprecedented non-monotonic dependence of T_N on P and showing that the local magnetic moment and/or magnetic configuration are only weakly perturbed by applied pressure $P \lesssim 24$ kbar. Our results support the preservation of a 4-in/4-out ground state across the whole accessed magnetic region of the electronic phase diagram.

Acknowledgements

We thank M. Vojta, J. van den Brink, L. Balents, Y. Ran and S. M. Disseler for useful discussions and A. Amato, R. Khasanov and H. Luetkens for technical support during the μ^+SR measurements. G. Prando acknowledges support by the Humboldt Research Fellowship for Postdoctoral researchers. G. Prando and B. Büchner acknowledge support by the Sonderforschungsbereich (SFB) 1143 project granted by the Deutsche Forschungsgemeinschaft (DFG). S. D. Wilson and M. J. Graf acknowledge support by NSF Grant No. DMR-1337567. R. Dally and S. D. Wilson acknowledge support by NSF CAREER Grant No. DMR-1056625. The experimental μ^+SR work was performed at the Swiss Muon Source (SμS) at the Paul Scherrer Institut, Switzerland.

Appendix A: Subtraction of the background signal from the PC

The design of the currently used PC is such that a dramatic reduction of the background signal is achieved which enables measurements of small and weakly magnetic samples. Still, we performed a detailed characterization of the empty PC magnetization within the same conditions of the real experiments for the aim of a quantitative and reliable disentanglement of the sample signal from the overall magnetic response. Representative steps of this procedure are shown in Fig. 7 and explained below in detail for both employed setups.

The magnetic behaviour of the empty pressure cell is presented in Fig. 7(a) and Fig. 7(b) for the specific cases of the $\varnothing = 0.8$ mm and $\varnothing = 0.4$ mm gaskets, respectively. Measurements have been performed upon the application of different F in order to check for the effects of gasket distortion on the overall magnetic response. Data have been approximated by an empirical function composed of one linear plus two exponential terms [see the continuous lines in Fig. 7(a) and Fig. 7(b)] and the extracted characteristic parameters have been used to properly interpolate for the required F values within the successive stages.

In the case of the $\varnothing = 0.8$ mm gasket and within the accessed experimental T range, the absolute variation of the signal from the sample is much stronger than that of the cell background. This can be observed by comparing Fig. 7(c) with Fig. 7(a). The subtraction of the linear term of the background contribution from the raw data (not shown) results in the full points reported in Fig. 7(c). Here, the empty points are the results of subtracting the two exponential terms as well (and, after proper normalization by the sample mass, these are presented in Fig. 3). The background contribution from the PC cannot be fully subtracted at low T values, as observed in Fig. 7(c). The actual reason is related to the employment of different gaskets for the background calibrations and the real measurements.

In the case of the $\varnothing = 0.4$ mm gasket the sample amount is smaller and, within the accessed experimental T range, the absolute variation of the signal from the sample is smaller than that of the cell background. This can be observed by comparing Fig. 7(d) with Fig. 7(b). This fact makes the subtraction procedure more delicate and, for this reason, two different approaches are followed.

The *procedure #1* is analogous to what is described above for the case of $\varnothing = 0.8$ mm gasket and it gives the results denoted by empty symbols in Fig. 7(d). However, small discrepancies between the signal from different gaskets (see above) may be critical.

Within *procedure #2*, ZFC (zero-field cooling) data are subtracted from the FC data with the advantage of carefully "cleaning" measurements from the cell contribution. This is expected to better account for the T dependence of the background if compared to what performed in procedure #1 as, in the current case, the signal *from the very same gasket* is being accounted for. Here we exploit the fact that the background term is not exhibiting any irreversible behaviour, i. e., differences between ZFC and FC branches. However, procedure #2 will also give a null result above the magnetic transition, where no ZFC/FC opening is observed. A linear contribution is then added to the result in order to match data from procedure #1 above the magnetic transition. We notice that this procedure, while not rigorous, can be applied to $Eu_2Ir_2O_7$ after considering its peculiar overall shape of the ZFC curve. In particular, it is observed that the ZFC branch can be approximately mimicked by a linear contribution over the whole accessed T range (from 2 K up to 300 K). The overall result of the subtraction procedure #2 is shown in Fig. 7(d) by full symbols.

As is shown, the discrepancies between the two methods are essentially irrelevant at relatively high temperatures, while the low-temperature side is still dominated by the differences between the gaskets used for calibration and for actual measurements. In Fig. 3, results from both the procedures have been used with the same meaning of symbols.

* E-mail: g.prando@ifw-dresden.de

[1] J. S. Gardner, M. J. P. Gingras, and J. E. Greedan, *Magnetic pyrochlore oxides*, Rev. Mod. Phys. **82**, 53 (2010).

[2] I. Kézsmárki, N. Hanasaki, K. Watanabe, S. Iguchi, Y. Taguchi, S. Miyasaka, and Y. Tokura, *Variation of the charge dynamics in bandwidth- and filling-controlled metal-insulator transitions of pyrochlore-type molybdates*, Phys. Rev. B **73**, 125122 (2006).

[3] G. Prando, P. Carretta, A. U. B. Wolter, R. Saint-Martin, A. Revcolevschi, and B. Büchner, *Amorphous ferromagnetism and re-entrant magnetic glassiness in single-crystalline $Sm_2Mo_2O_7$*, Phys. Rev. B **90**, 085111 (2014) and references therein.

[4] D. Yanagishima and Y. Maeno, *Metal-Nonmetal Changeover in Pyrochlore Iridates*, J. Phys. Soc. Jpn. **70**, 2880 (2001).

[5] K. Matsuhira, M. Wakeshima, Y. Hinatsu, and S. Takagi, *Metal-Insulator Transitions in Pyrochlore Oxides $Ln_2Ir_2O_7$*, J. Phys. Soc. Jpn. **80**, 094701 (2011).

[6] W. Witczak-Krempa, G. Chen, Y. B. Kim, and L. Balents, *Correlated Quantum Phenomena in the Strong Spin-Orbit Regime*, Annu. Rev. Condens. Matter Phys. **5**, 57 (2014).

[7] H. Takatsu, K. Watanabe, K. Goto, and H. Kadowaki, *Comparative study of low-temperature x-ray diffraction experiments on $R_2Ir_2O_7$ (R = Nd, Eu, and Pr)*, Phys. Rev. B **90**, 235110 (2014).

[8] T. Katsufuji, H. Y. Hwang, and S.-W. Cheong, *Anomalous Magnetotransport Properties of $R_2Mo_2O_7$ near the Magnetic Phase Boundary*, Phys. Rev. Lett. **84**, 1998 (2000).

[9] Y. Moritomo, S. Xu, A. Machida, T. Katsufuji, E. Nishibori, M. Takata, M. Sakata, and S.-W. Cheong, *Chemical pressure control of exchange interaction in Mo pyrochlore*, Phys. Rev. B **63**, 144425 (2001).

[10] N. Hanasaki, K. Watanabe, T. Ohtsuka, I. Kézsmárki, S. Iguchi, S. Miyasaka, and Y.Tokura, *Nature of the Transition between a Ferromagnetic Metal and a Spin-Glass Insulator in Pyrochlore Molybdates*, Phys. Rev. Lett. **99**, 086401 (2007).

[11] K. Ueda, J. Fujioka, C. Terakura, and Y. Tokura, *Pressure and magnetic field effects on metal-insulator transitions of bulk and domain wall states in pyrochlore iridates*, Phys. Rev. B **92**, 121110 (2015).

[12] X. Wan, A. M. Turner, A. Vishwanath, and S. Y. Savrasov, *Topological semimetal and Fermi-arc surface states in the*

electronic structure of pyrochlore iridates, Phys. Rev. B **83**, 205101 (2011).

[13] W. Witczak-Krempa and Y. B. Kim, *Topological and magnetic phases of interacting electrons in the pyrochlore iridates*, Phys. Rev. B **85**, 045124 (2012).

[14] W. Witczak-Krempa, A. Go, and Y. B. Kim, *Pyrochlore electrons under pressure, heat, and field: Shedding light on the iridates*, Phys. Rev. B **87**, 155101 (2013).

[15] H. Sagayama, D. Uematsu, T. Arima, K. Sugimoto, J. J. Ishikawa, E. O'Farrell, and S. Nakatsuji, *Determination of long-range all-in-all-out ordering of Ir^{4+} moments in a pyrochlore iridate $Eu_2Ir_2O_7$ by resonant x-ray diffraction*, Phys. Rev. B **87**, 100403(R) (2013).

[16] S. M. Disseler, *Direct evidence for the all-in/all-out magnetic structure in the pyrochlore iridates from muon spin relaxation*, Phys. Rev. B **89**, 140413(R) (2014).

[17] A. B. Sushkov, J. B. Hofmann, G. S. Jenkins, J. Ishikawa, S. Nakatsuji, S. Das Sarma, and H. D. Drew, *Optical evidence for a Weyl semimetal state in pyrochlore $Eu_2Ir_2O_7$*, arXiv:1507.01038 (2015).

[18] H. Ishikawa, S. Xu, Y. Moritomo, A. Nakamura, Y. Ohishi, and K. Kato, *High-pressure structural investigation of ferromagnetic $Nd_2Mo_2O_7$*, Phys. Rev. B **70**, 104103 (2004).

[19] A. Apetrei, I. Mirebeau, I. Goncharenko, D. Andreica, and P. Bonville, *Microscopic Study of a Pressure-Induced Ferromagnetic–Spin-Glass Transition in the Geometrically Frustrated Pyrochlore $(Tb_{1-x}La_x)_2Mo_2O_7$*, Phys. Rev. Lett. **97**, 206401 (2006).

[20] I. Mirebeau, A. Apetrei, I. Goncharenko, D. Andreica, P. Bonville, J. P. Sanchez, A. Amato, E. Suard, and W. A. Crichton, *Pressure-induced ferromagnet to spin-glass transition in $Gd_2Mo_2O_7$*, Phys. Rev. B **74**, 174414 (2006).

[21] S. Iguchi, N. Hanasaki, M. Kinuhara, N. Takeshita, C. Terakura, Y. Taguchi, H. Takagi, and Y. Tokura, *Emergence of a Diffusive Metal State with No Magnetic Order near the Mott Transition in Frustrated Pyrochlore-Type Molybdates*, Phys. Rev. Lett. **102**, 136407 (2009).

[22] M. Sakata, T. Kagayama, K. Shimizu, K. Matsuhira, S. Takagi, M. Wakeshima, Y. Hinatsu, *Suppression of metal-insulator transition at high pressure and pressure-induced magnetic ordering in pyrochlore oxide $Nd_2Ir_2O_7$*, Phys. Rev. B **83**, 041102(R) (2011).

[23] F. F. Tafti, J. J. Ishikawa, A. McCollam, S. Nakatsuji, and S. R. Julian, *Pressure-tuned insulator to metal transition in $Eu_2Ir_2O_7$*, Phys. Rev. B **85**, 205104 (2012).

[24] H. Shinaoka, S. Hoshino, M. Troyer, and P. Werner, *Phase Diagram of Pyrochlore Iridates: All-in–All-out Magnetic Ordering and Non-Fermi-Liquid Properties*, Phys. Rev. Lett. **115**, 156401 (2015).

[25] W. Schottenhamel, *Aufbau eines hochauflösenden Dilatometers und einer hydrostatischen SQUID-Druckzelle sowie Untersuchungen an korrelierten Übergangsmetalloxiden*, Ph. D. Thesis, Technische Universität Dresden (2015 – submitted).

[26] P. L. Alireza and G. G. Lonzarich, *Miniature anvil cell for high-pressure measurements in a commercial superconducting quantum interference device magnetometer*, Rev. Sci. Instr. **80**, 023906 (2009).

[27] G. J. Piermarini, S. Block, and J. D. Barnett, *Hydrostatic limits in liquids and solids to* 100 *kbar*, J. Appl. Phys. **44**, 5377 (1973).

[28] M. Clark and T. Smith, *Pressure dependence of T_c for lead*, J. Low Temp. Phys. **32**, 495 (1978).

[29] S. J. Blundell, *Spin-polarized muons in condensed matter physics*, Contemp. Phys. **40**, 175 (1999).

[30] A. Yaouanc, P. Dalmas de Réotier, *Muon Spin Rotation, Relaxation, and Resonance: Applications to Condensed Matter* (Oxford University Press, Oxford, 2011).

[31] See Supplemental Material, which also includes Refs. 32–37, for detailed information about the analysis of ZF-μ^+SR data and about the magnetic characterization of the sample by means of ambient-pressure electrical resistivity, ZF-μ^+SR and dc magnetization.

[32] G. Prando, P. Bonfà, G. Profeta, R. Khasanov, F. Bernardini, M. Mazzani, E. M. Brüning, A. Pal, V. P. S. Awana, H.-J. Grafe, B. Büchner, R. De Renzi, P. Carretta, and S. Sanna, *Common effect of chemical and external pressures on the magnetic properties of RCoPO (R = La, Pr)*, Phys. Rev. B **87**, 064401 (2013).

[33] G. Prando, G. Profeta, A. Continenza, R. Khasanov, A. Pal, V. P. S. Awana, B. Büchner, and S. Sanna, *Common effect of chemical and external pressures on the magnetic properties of RCoPO (R = La, Pr, Nd, Sm). II.*, Phys. Rev. B **92**, 144414 (2015).

[34] S. Zhao, J. M. Mackie, D. E. MacLaughlin, O. O. Bernal, J. J. Ishikawa, Y. Ohta, and S. Nakatsuji, *Magnetic transition, long-range order, and moment fluctuations in the pyrochlore iridate $Eu_2Ir_2O_7$*, Phys. Rev. B **83**, 180402(R) (2011).

[35] G. Prando, O. Vakaliuk, S. Sanna, G. Lamura, T. Shiroka, P. Bonfà, P. Carretta, R. De Renzi, H.-H. Klauss, C. G. F. Blum, S. Wurmehl, C. Hess, and B. Büchner, *Role of in-plane and out-of-plane dilution in CeFeAsO: Charge doping versus disorder*, Phys. Rev. B **87**, 174519 (2013).

[36] N. Taira, M. Wakeshima, and Y. Hinatsu, *Magnetic properties of iridium pyrochlores $R_2Ir_2O_7$ (R = Y, Sm, Eu and Lu)*, J. Phys.: Cond. Matt. **13**, 5527 (2001).

[37] J. J. Ishikawa, E. C. T. O'Farrell, and S. Nakatsuji, *Continuous transition between antiferromagnetic insulator and paramagnetic metal in the pyrochlore iridate $Eu_2Ir_2O_7$*, Phys. Rev. B **85**, 245109 (2012).

[38] In particular, the observed behaviour may be associated with the two experimental setups employed for dc magnetization measurements, as discussed in Ref. 31. This issue is currently still not completely understood and will be the subject of further experimental investigation.

[39] S. M. Disseler, C. Dhital, A. Amato, S. R. Giblin, C. de la Cruz, S. D. Wilson, and M. J. Graf, *Magnetic order in the pyrochlore iridates $A_2Ir_2O_7$ (A = Y, Yb)*, Phys. Rev. B **86**, 014428 (2012).

[40] G. Prando *et al.*, manuscript under preparation.

[41] J. S. Möller, P. Bonfà, D. Ceresoli, F. Bernardini, S. J. Blundell, T. Lancaster, R. De Renzi, N. Marzari, I. Watanabe, and S. Sulaiman, *Playing quantum hide-and-seek with the muon: localizing muon stopping sites*, Phys. Scr. **88**, 068510 (2013).

[42] P. Bonfà, F. Sartori, and R. De Renzi, *Efficient and reliable strategy for identifying muon sites based on the double adiabatic approximation*, J. Phys. Chem. C **119**, 4278 (2015).

[43] G. Chen and M. Hermele, *Magnetic orders and topological phases from $f-d$ exchange in pyrochlore iridates*, Phys. Rev. B **86**, 235129 (2012).

[44] Y. Yamaji and M. Imada, *Metallic Interface Emerging at Magnetic Domain Wall of Antiferromagnetic Insulator: Fate of Extinct Weyl Electrons*, Phys. Rev. X **4**, 021035 (2014).